Bioorganic Chemistry 119 (2022) 105505

Contents lists available at ScienceDirect

Bioorganic Chemistry

journal homepage: www.elsevier.com/locate/bioorg

A novel Cereblon E3 ligase modulator with antitumor activity in gastrointestinal cancer

Svenja Lier [a,1], Andreas Sellmer [b,1], Felix Orben [a], Stephanie Heinzlmeir [c], Lukas Krauß [a], Christian Schneeweis [a], Zonera Hassan [a], Carolin Schneider [a], Arlett Patricia Gloria Schäfer [a], Herwig Pongratz [b], Thomas Engleitner [d], Rupert Öllinger [d], Anna Kuisl [e], Florian Bassermann [e,f], Christoph Schlag [a], Bo Kong [g,h], Stefan Dove [b], Bernhard Kuster [c,f,i], Roland Rad [d,f], Maximilian Reichert [a,f,j], Matthias Wirth [k], Dieter Saur [f,l], Siavosh Mahboobi [b,*], Günter Schneider [a,m,*]

[a] Medical Clinic and Policlinic II, Klinikum Rechts der Isar, TU Munich, 81675 Munich, Germany
[b] Institute of Pharmacy, Faculty of Chemistry and Pharmacy, University of Regensburg, 93040 Regensburg, Germany
[c] Chair of Proteomics and Bioanalytics, TU Munich, 85354 Freising, Germany
[d] Institute of Molecular Oncology and Functional Genomics, MRI, TU Munich, Germany
[e] Medical Clinic and Policlinic III, Klinikum Rechts der Isar, TU Munich, 81675 Munich, Germany
[f] German Cancer Research Center (DKFZ) and German Cancer Consortium (DKTK), 69120 Heidelberg, Germany
[g] Department of Surgery, Klinikum Rechts der Isar, TU Munich, 81675 Munich, Germany
[h] Department of General Surgery, University of Ulm, 89081 Ulm, Germany
[i] Bavarian Center for Biomolecular Mass Spectrometry (BayBioMS), TU Munich, 85354 Freising, Germany
[j] Center for Protein Assemblies (CPA), Technische Universität München, 85747 Garching, Germany
[k] Department of Hematology, Oncology and Cancer Immunology, Campus Benjamin Franklin, Charité – Universitätsmedizin Berlin, 12203 Berlin, Germany
[l] Institute for Translational Cancer Research and Experimental Cancer Therapy, Klinikum Rechts der Isar, TU Munich, Germany
[m] University Medical Center Göttingen, Department of General, Visceral and Pediatric Surgery, 37075 Göttingen, Germany

ARTICLE INFO

Keywords:
Cereblon
GSPT1
GSPT2
MYC
PLK1

ABSTRACT

Targeted protein degradation offers new opportunities to inactivate cancer drivers and has successfully entered the clinic. Ways to induce selective protein degradation include proteolysis targeting chimera (PROTAC) technology and immunomodulatory (IMiDs) / next-generation Cereblon (CRBN) E3 ligase modulating drugs (CELMoDs). Here, we aimed to develop a MYC PROTAC based on the MYC-MAX dimerization inhibitor 10058-F4 derivative 28RH and Thalidomide, called MDEG-541. We show that a subgroup of gastrointestinal cancer cell lines and primary patient-derived organoids are MDEG-541 sensitive. Although MYC expression was regulated in a CRBN-, proteasome- and ubiquitin-dependent manner, we provide evidence that MDEG-541 induced the degradation of CRBN neosubstrates, including G1 to S phase transition 1/2 (GSPT1/2) and the Polo-like kinase 1 (PLK1). In sum, we have established a CRBN-dependent degrader of relevant cancer targets with activity in gastrointestinal cancers.

1. Introduction

Targeted protein degradation is a powerful tool to eliminate cancer drivers and will tremendously expand the spectrum of cancer targets [1–4]. Principles allowing to degrade proteins with various degrees of specificity have expanded in the last years. Prominent examples include the proteolysis targeting chimera (PROTAC) technology and immunomodulatory (IMiDs) / next-generation Cereblon (CRBN) E3 ligase

* Corresponding authors at: University Medical Center Göttingen, Department of General, Visceral and Pediatric Surgery, 37075 Göttingen and Klinikum rechts der Isar, Technische Universität München, 81675 Munich, Germany (G. Schneider). Institute of Pharmacy, Faculty of Chemistry and Pharmacy, University of Regensburg, 93040 Regensburg, Germany (S. Mahboobi).
E-mail addresses: siavosh.mahboobi@ur.de (S. Mahboobi), guenter.schneider@med.uni-goettingen.de (G. Schneider).
[1] Equally contributing first authors.

https://doi.org/10.1016/j.bioorg.2021.105505
Received 22 June 2021; Received in revised form 6 October 2021; Accepted 17 November 2021
Available online 20 November 2021

modulating drugs (CELMoDs).

The proteolysis targeting chimera (PROTAC) technology provides the opportunity to address "undruggable" therapeutic cancer targets [1,4]. This class of drugs induces a trimeric complex between the target of interest, the PROTAC, and an E3 ubiquitin ligase, leading to the ubiquitination of the target and its proteasomal degradation [1,4]. Proteins targeted by the PROTAC technology are often degraded in a short time-frame of only a few hours, reveal immense potency due to a catalytic mode of action, and a very high specificity is demonstrated for some PROTACs [1,5–7]. Although the number of E3 ubiquitin ligases used in PROTAC concepts is expanding, currently von Hippel-Lindau (VHL) and CRBN E3 ligases are most frequently used. The PROTAC technology entered clinical testing in breast and prostate cancer (NCT04072952, NCT03888612).

The immunomodulatory (IMiDs) drugs thalidomide, lenalidomide, or pomalidomide are approved in the clinic for the treatment of multiple myeloma and myelodysplastic syndrome (MDS) with deletion of chromosome 5q [2]. This class of drugs acts via the CUL4-RBX1-DDB1-CRBN ($CRL4^{CRBN}$) E3 ligase by acting as molecular glue degrader to scaffold protein-protein interactions [2]. Binding to the receptor subunit of the E3 ligase, CRBN, induces the ubiquitination and degradation of neo-substrates like Ikaros (IKZF1) and Aiolos (IKZF3) [8,9] or CK1α [10], relevant for the therapeutic efficacy in multiple myeloma or MDS, respectively. Various CELMoDs are currently under development [2,11].

The Myelocytomatosis oncogene (MYC) is a relevant therapeutic target in cancer [12,13] and acts through heterodimerization with the MYC associated factor X (MAX) to regulate genes needed for growth and proliferation [12,13]. Direct targeting of MYC remains challenging [13,14]. In this study, we aimed at developing a MYC PROTAC degrader based on the MYC-MAX dimerization inhibitor 10058-F4 [15] derivative 28RH linked to the CRBN-binder Thalidomide [16]. We characterized one compound, MDEG-541, with activity in gastrointestinal cancers. Although MDEG-541 regulates MYC in a fashion dependent on CRBN, ubiquitination, and the proteasome, the compound acts pleiotropic and also decreased the expression of G1 To S Phase Transition 1 (GSPT1), GSPT2, and the Polo-like kinase 1 (PLK1).

2. Material and methods

2.1. Compounds

MG132 (M8699), Bortezomib (5043140001), and Thalidomide (T144) were purchased from Sigma-Aldrich (Munich, Germany). TAK-243 (S8341) and 10058-F4 (S7153) were purchased from Selleckchem (Munich, Germany). CC-885 (HY-101488), Volasertib (BI 6727), and ARV-771 was purchased from MedChemExpress, CC-90009 (207005) was purchased from MedKoo.

2.2. Synthesis of MDEG-541

Detailed synthesis of MDEG-541 and compound 619 can be found in supplemental methods (SM).

2.3. Cell culture

Cells were cultured in either Dulbecco's Modified Eagle's Medium (DMEM, Sigma-Aldrich, Munich, Germany) (HCT116 RRID:CVCL_0291, HPAC RRID:CVCL_3517, HUPT3 RRID:CVCL_1299, KP-4 RRID:CVCL_8727, MIA PaCa-2 RRID:CVCL_0428, PANC-1 RRID:CVCL_0480, PATU8988S RRID:CVCL_1846, PATU8988T RRID:CVCL_1847, SW480 RRID:CVCL_0546, SW707 RRID:CVCL_6230, T84 RRID:CVCL_0555) or RPMI 1640-GlutaMAX™ Medium (Thermo Fisher Scientific, Munich, Germany)(BxPC-3 RRID:CVCL_0186, COLO320 RRID:CVCL_1989, DANG RRID:CVCL_0243, HT-29 RRID:CVCL_0320, NCI-H716 RRID:CVCL_1581, PSN1 RRID:CVCL_1644) supplemented with 10% (v/v) fetal bovine serum (FBS, Merck, Darmstadt, Munich) and 1 % (v/v) Penicillin/Streptomycin (Thermo Fisher Scientific, Munich, Germany). Sub-culturing, Mycoplasma testing, and authentication is described in SM.

2.4. Protein lysates and immunoblotting

Cell lysis, immunoblotting, antibodies and dilutions are described in SM. Immunoblots were visualized using the Odyssey Fc Imaging System (RRID:SCR_015795) (Li-cor Biosciences GmbH, Germany) and quantified with the Image J software (RRID:SCR_003070) (NIH, Bethesda, MD, USA).

2.5. Proteomics, LC-MS^3 analysis, Peptide and protein identification and quantification, and Proteome data analysis

A detailed description can be found in SM.

2.6. Data availability

The mass spectrometry proteomics data and complete MaxQuant (RRID:SCR_014485) search results have been deposited to the ProteomeXchange Consortium (RRID:SCR_004055) (http://www.proteomexchange.org/) via the PRIDE partner repository (RRID:SCR_003411) with the data set identifier: PXD018674. RNA-seq data of MDEG-541, 10058-F4, or Thalidomide treated HCT116 cells are deposited in European Nucleotide Archive (ENA): PRJEB42732.

2.7. Cell viability assay, dose response, GI_{50} calculation, colony formation assay

For clonogenic assays, PSN1 (250 cells/well) and HCT116 (200 cells/well) cells were seeded in a 24-well plate. The cells were treated in technical triplicates with several concentrations of the compounds of interest and the corresponding vehicle controls. After ten (HCT116 cells) or twelve days (PSN1 cells), the supernatant was removed and the treated cells were washed (2x) with PBS, fixed and stained with a 0.4 % (w/v) crystal violet solution (Sigma-Aldrich, Munich, Germany) for 30 min. Cells were washed with water and airdried. The crystal violet staining was dissolved under shaking in 200 µL of 1 % (w/v) sodium dodecyl sulfate (SDS, Serva, Rosenheim, Germany) and absorbance was measured with a microplate reader at 565 nm (BMG Labtech, Champigny-sur-Marne, France).

For MTT assays, cells were treated for 72 h in a 96-well (Thermo Fisher Scientific, Munich, Germany) plate with MDEG-541 using a 7-point or 12-point dilution ranging from 50 µM to 0.78 µM or 48 nM, respectively and DMSO as vehicle control. 10 µL Thiazolyl Blue Tetrazolium Bromide (5 mg/ml) (MTT, Sigma-Aldrich, Munich, Germany) reagent was added to each well and incubated for 4 h at 37 °C. Afterwards medium was removed and the formazan crystals was dissolved in 200 µL Dimethyl sulfoxide (DMSO):EtOH (1:1 v/v), incubated for five minutes on a horizontal shaker and absorbance was measured at 595 nm using a Multiskan plate reader (Thermo Fisher Scientific, Munich, Germany). The growth inhibitory dose 50% (GI_{50}) was calculated with GraphPad Prism 5 (RRID:SCR_002798) by non-linear regression of the log transformed data with the log(inhibitor) vs. normalized response-variable slope tool.

2.8. RNA-seq and GSEA

For GSEA a rlog normalized expression matrix was used to perform a GSEA using the GeneTrail 3.0 web tool with default settings [17]. The drug sensitivity of human pancreatic cancer and colon carcinoma cell lines (n = 17) to MDEG-541 was determined and the GI_{50} values were correlated with the gene expression obtained by RNA-seq in the Cancer Cell Line Encyclopedia (RRID:SCR_007073) (CCLE, CCLE_expression_full.csv, February 2020, https://depmap.org/portal/downl

oad) [18]. The CCLE gene expression was quantified as log2 transcripts per million following the GTEx pipeline of the Broad Institute and correlated with the GI_{50} values using Spearman methods. RNA-seq is detailed described in SM.

2.9. Patient derived organoids and analysis of MDEG-541 responsiveness, human fibroblasts

Patient samples were received from endoscopy punctures or surgical resection. Organoid models were established and analyzed in accordance with the declaration of Helsinki, were approved by the local ethical committee (Project 207/15), and written informed consent from

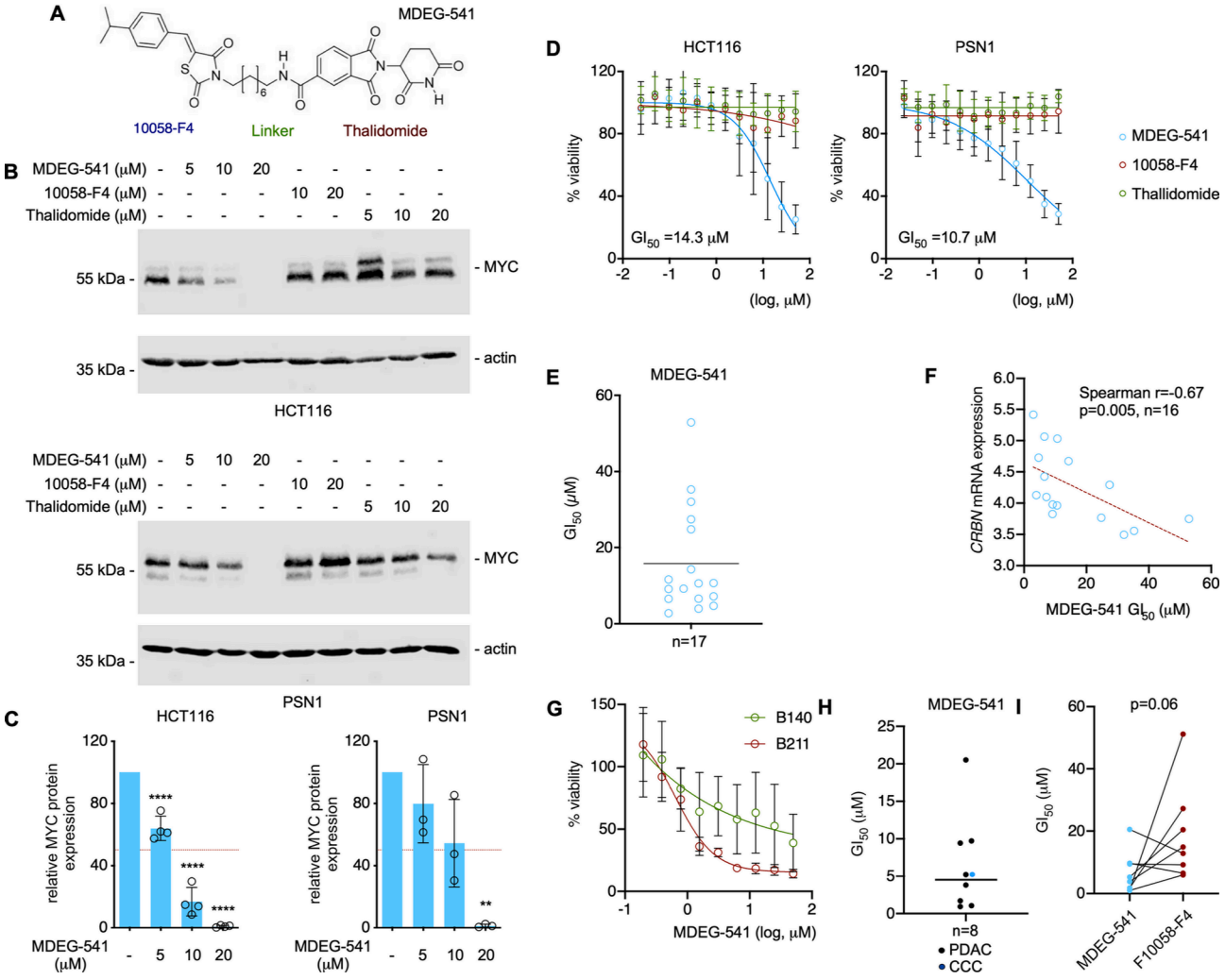

Fig. 1. *MDEG-541 reduces MYC expression dependent on ubiquitination, the proteasome, and Cereblon and is active in a subtype of gastrointestinal cancers* A Chemical Structure of MDEG-541 with the 10058-F4 moiety linked to the thalidomide moiety. B, C B MYC western blot of HCT116 (upper panel) or PSN1 (lower panel) cells treated for 24 h with the indicated concentrations of MDEG-541 (5 μM, 10 μM, 20 μM), 10058-F4 (10 μM, 20 μM), Thalidomide (5 μM, 10 μM, 20 μM), or DMSO vehicle control. Actin: loading control. C Quantification of four (HCT116, left panel) or three (PSN1, right panel) independent biological experiments corresponding to B. Lines mark 50% expression. p-value of an ANOVA: $^{**}p < 0.01$, $^{****}p < 0.0001$. D HCT116 (left panel) and PSN1 (right panel) cells were treated for 72 h with 50 μM, 25 μM, 12.5 μM, 6.25 μM, 3.125 μM, 1.56 μM, 0.78 μM, 0.39 μM, 0.19 μM, 0.098 μM, and 0.049 μM of MDEG-541, 10058-F4, Thalidomide or were left as DMSO treated vehicle controls. Viability was measured with MTT assays and vehicle treated controls were arbitrarily set to 100%. GI_{50} values calculated by a non-linear regression are depicted. Experiment was performed in five (PSN1) and six (HCT116) biological replicates conducted as technical triplicates. Shown is the mean ± S.D. E The growth inhibitory concentration 50% (GI_{50}) was determined in 17 human colon and pancreatic cancer cell lines. In 15 cell lines a twelve-point two-fold MDEG-541 dilution (range: 50 μM-0.048 μM) was used. In two lines a seven-point two-fold MDEG-541 dilution (range: 50 μM-0.78 μM) was used. With the exception of COLO320 in which two biological replicates done as technical triplicates were analyzed, data are based on at least three biological replicates performed as technical triplicates. PDAC cell lines: BxPC-3, DANG, HPAC, HUPT3, KP4, MIA PaCa-2, Panc-1, PATU8988S, PATU8988T, PSN1. Colon cancer cell lines: COLO320, HCT116, HT-29, NCI-H716, SW480, SW707, T84. MTT was used to determine the viability. The mean GI_{50} of the 17 cell lines is indicated by a line. F *Cereblon* mRNA expression was correlated with the GI_{50} values in 16 human colon and pancreatic cancer cell lines. The Spearman r and the p value are indicated. G Representative MDEG-541 dose response curves of two pancreatic cancer organoids treated with 50 μM, 25 μM, 12.5 μM, 6.25 μM, 3.125 μM, 1.56 μM, 0.78 μM, 0.39 μM, and 0.19 μM MDEG-541 as indicated or DMSO vehicle control over 72 h. CellTiter-Glo® assays were used to determine the dose-response. Three independent biological experiments performed as technical triplicates were analyzed. Shown is the mean ± SD. H, I The GI_{50} of MDEG-541 and 10058-F4 was determined in eight gastrointestinal cancer organoids as illustrated in G. CellTiter-Glo® assays were used to determine the dose-response of a nine-point MDEG-541 or 10058-F4 dilution (range: 50–0.78 μM). Cells were treated for 72 h. Three biological replicates conducted as technical triplicates were analyzed. H GI_{50} values in pancreatic cancer organoids (black dots) and one cholangiocellular carcinoma organoid (blue dot). The mean GI_{50} of all organoids was indicated by a line. I GI_{50} of MDEG-541 was compared to the 10058-F4 GI_{50} in eight gastrointestinal cancer organoids. The mean was compared by an unpaired *t*-test and the p-value is indicated. (For interpretation of the references to color in this figure legend, the reader is referred to the web version of this article.)

the patients for research use was obtained prior to the investigation. A detailed description of organoid culturing and determination of the drug response can be found in SM. Isolation and propagation of human cancer-associated fibroblast is described in SM.

2.10. Generation of CRBN deficient cell lines

Described in SM.

2.11. Gene Effect Ceres Scores and CRBN protein expression

The Ceres scores for *GSPT1* (CRISPR AVANA PUBLIC 20Q4) and CRBN protein expression (Proteomics) were accessed via the DepMap portal [19].

2.12. Statistical analysis

At least three biological replicates were performed for each experiment if not assigned otherwise. The data were analyzed with GraphPad Prism 5/8 software unless otherwise indicated. Data are shown as mean values ± SD. Analysis of Variance (ANOVA) or two-sided *t*-test was used to determine statistically significance as indicated. Multiple testing was corrected according to Bonferroni.

3. Results

3.1. Synthesis of 10058-F4-Thalidomide compounds

To link the MYC-MAX dimerization inhibitor 10058-F4 substructure of 28RH with the Cereblon-binder Thalidomide we built the heterocyclic ring system of 10058-F4 derivative 28RH up by ultrasonic-assisted condensation of a mono-Boc protected diamine with carbon disulfide, ethyl 2-chloroacetate and a suitable substituted benzaldehyde. In the following the Boc-group was cleaved by use of trifluoroacetic acid. To introduce the Thalidomide-substructure, we performed a BOP-mediated amidation of the resulting amine with the carboxylic acid 7 (SFig. 1), exemplified for the MDEG-541 compound. We screened several compounds, including lenalidomide- or pomalidomide-based compounds, according to cellular activity and regulation of MYC expression. MDEG-541 was selected by these data and we characterized MDEG-541 as a potential PROTAC in more detail (Fig. 1A).

3.2. MDEG-541 regulates MYC protein expression dependent on the proteasome, Cereblon and ubiquitination

To test the effects of MDEG-541 on MYC protein expression, we used the MYC-amplified colon cancer line HCT116 and the MYC-amplified pancreatic cancer line PSN1. Twenty-four hours after MDEG-541 treatment with the indicated concentrations, we detected a dose-dependent decrease of MYC protein expression (Fig. 1B and 1C). Neither the dimerization inhibitor nor Thalidomide affected MYC protein expression (Fig. 1B). In order to demonstrate the dependency of the MYC degradation on the proteasome, we used the proteasome inhibitors Bortezomib and MG-132. Both proteasome inhibitors rescued the MDEG-541-induced downregulation of MYC (SFig. 2A). To further corroborate the involvement of the ubiquitin-proteasome system, we used the ubiquitination inhibitor TAK-243 [20]. Co-treatment of cells with MDEG-541 and TAK-243, again, rescued the downregulation of MYC (SFig. 2B). To elaborate the kinetic, we investigated MDEG-541 effects over time. For a PROTAC approach, we observed delayed kinetics, with decreased MYC levels after 10 h (SFig. 2C). We generated CRBN knock-out clones, to demonstrate the dependency of the MDEG-541 action on the E3 ligase (SFig. 2D and 2E). In these genetic models, decreased MYC expression induced by MDEG-541 was blocked in *CRBN*-deficient PSN1 and HCT116 cells (SFig. 2D and 2E). In sum, the data showed that MDEG-541 induced downregulation of MYC protein expression in a ubiquitin-, proteasome-, and Cereblon-dependent fashion.

3.3. Efficacy of MDEG-541 in cell lines and primary patient-derived organoid models

To analyze cellular effects of MDEG-541, we determined the viability of HCT116 and PSN1 in response to MDEG-541 treatment. A dose-dependent reduction of the viability was observed with a half-maximal growth inhibitory concentration (GI_{50}) of 14.3 μM in HCT116 and 10.7 μM in PSN1 cells (Fig. 1D). The response to 10058-F4 was marginal in the investigated dose range and Thalidomide did not affect the viability at all (Fig. 1D). Clonogenic growth was also significantly reduced by MDEG-541 in a dose-dependent fashion in both cell lines (SFig. 3A). MDEG-541 outperformed 10058-F4 and Thalidomide in the investigated dose ranges (SFig. 3A). To evaluate the responsiveness to MDEG-541, we determined dose response curves in 17 cancer cell lines, with a focus on colon and pancreatic cancer cell lines. GI_{50} values ranging from approximately 3 μM to 50 μM were observed (Fig. 1E). Compared to other potent PROTACs, like the BRD4 degrader ARV771 [21], which reduced MYC expression (SFig. 3B), the GI_{50} values of MDEG-541 are high (SFig. 3C). Aiming to find potential biomarkers for MDEG-541 sensitivity, we correlated the GI_{50} values to mRNA expression in the investigated cell lines (STable1). Interestingly, the MDEG-541 GI_{50} was correlated to *CRBN* mRNA (Fig. 1F and STable1) and protein (SFig. 3D), furthermore pointing to a CRBN-dependent mode of action. Furthermore, this observation might contribute to the different sensitivity of cancer cells to MDEG-541.

Next, we used patient-derived cholangiocarcinoma and pancreatic cancer organoids, which have shown predictive power for the response of gastrointestinal cancers in the clinic [22]. These organoids differed fundamentally in the MDEG-541 responsiveness. The dose response of a sensitive (B211, pancreatic cancer) and a rather resistant (B140, pancreatic cancer) organoid is depicted in Fig. 1G. A range of GI_{50} values from 0.97 μM in the most sensitive organoid to 20.5 μM in the most resistant one could be observed (Fig. 1H). In contrast to classical adherent cell lines, the dimerization inhibitor 10058-F4 was more potent in the 3D organoid models (Fig. 1I), which could probably be due to cultivation conditions, among other factors, and requires further investigation. However, for most organoids, the MDEG-541 GI_{50} was still lower than the 10058-F4 GI_{50} value (Fig. 1I) corresponding to a reduced mean MDEG-541 GI_{50} value (mean GI_{50} MDEG-541: 6.5 μM, mean GI_{50} 10058-F4: 18.5 μM, unpaired *t*-test: $p = 0.06$) in the organoid models. This observation showed an increased potency of MDEG-541 versus the dimerization inhibitor. In addition, we used primary human fibroblast to evaluate the potential therapeutic window. In two fibroblast lines, GI_{50} was above 60 μM (SFig. 3E). Compared to the single-digit μM activity in sensitive cancer lines, these data at least point to an existing therapeutic window.

3.4. MDEG-541 mode of action

To unbiasedly find pathways affected by MDEG-541, we performed RNA-seq in HCT116 cells, which were treated for 12 h with MDEG-541, 10058-F4, or Thalidomide. Thalidomide and 10058-F4 demonstrated no effects on cell viability at the concentrations used (Fig. 1D). Since MDEG-541 contains the 10058-F4 and Thalidomide warheads, we compared RNA expression profiles of MDEG-541 treated cells with profiles of Thalidomide treated cells or profiles of 10058-F4 treated cells by gene set enrichment analysis (GSEA) using the GeneTrail 3.0 [17] web tool and the HALLMARK gene signatures [23]. In an overlap analysis of both GSEAs, we detected 15 significantly enriched/depleted signatures (Fig. 2A). Prominent MDEG-541 inhibited pathways included cell cycle pathways, specifically the pro-proliferative E2F transcription factor, DNA repair and the MYC network (Fig. 2B), underpinning that MDEG-541 targets MYC. Stress responsive pathways, for instance TNFα-NFκB signaling, were activated by MDEG-541 treatment (Fig. 2B). In

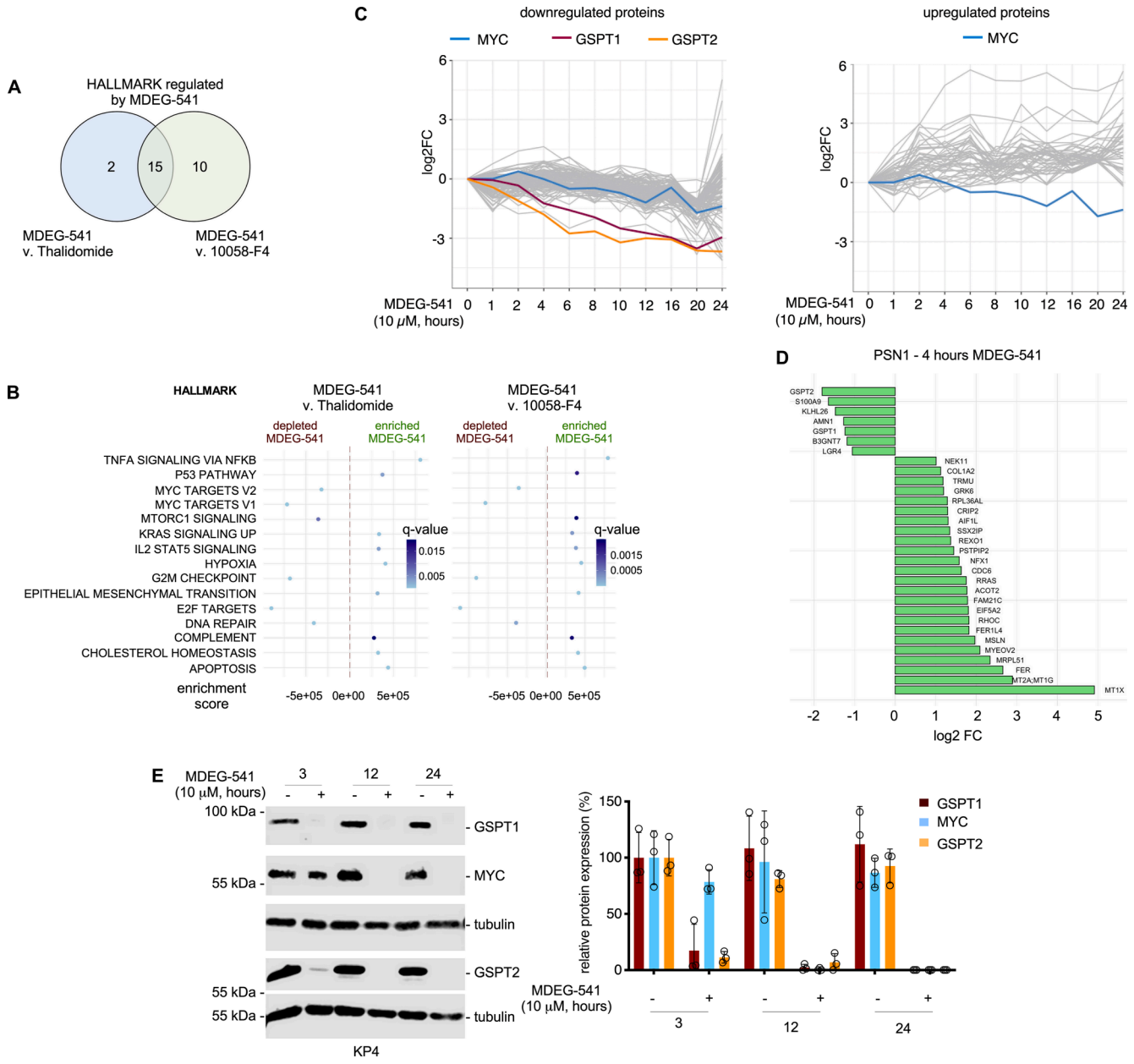

Fig. 2. *MDEG-541 regulated mRNAs and proteins* A, B A HCT116 cells were treated with MDEG-541, 10058-F4, or Thalidomide (10 μM each, 12 h). RNA-seq data were analyzed with a GSEA using the GeneTrail 3.0 web tool with the HALLMARK signatures of the MolSigDB. The MDEG-541 treatment was compared to the 10058-F4 and Thalidomide treatments, respectively. Venn diagram of signatures regulated in both comparisons with a $q < 0.05$. B Depiction of the 15 HALMARK signatures of A, significantly regulated by MDEG-541 in both comparisons. q-value is color coded, the enrichment score (ES) is blotted at the x-axis. C Mass spectrometry measurement of protein expression in response to MDEG-541 treatment (10 μM) over the indicated time points and untreated control. Shown are the upregulated proteins (right panel) and downregulated proteins (left panel) with a significant fold change at 20 h and the expression change over all time points. MYC (blue lines), GSPT1 (red line), GSPT2 (orange line) are depicted. D Proteins from A regulated with a log2 FC $> \pm 1$ at four hours after the treatment with 10 μM MDEG-541. E The pancreatic cancer cell line KP4 was treated for 3 h, 12 h or 24 h with 10 μM MDEG-541 or DMSO as a vehicle control. Left panel: western blot detected the expression GSPT1, MYC, and GSPT2. Tubulin: loading control. Right panel: Quantification of three independent experiments. Paired *t* test: *$p < 0.05$, **$p < 0.01$. (For interpretation of the references to color in this figure legend, the reader is referred to the web version of this article.)

sum, these data demonstrate that cancer-relevant pathways were blocked by MDEG-541.

We used Tandem Mass Tag (TMT) mass spectrometry to determine the effects of MDEG-541 treatment on the proteome in PSN1 cells. Corresponding to the kinetics by which MDEG-541 downregulated MYC as determined by western blotting (SFig. 2C), MYC protein was decreased 10 h after MDEG-541 treatment (blue line) (Fig. 2C). To find proteins which might be more directly regulated by MDEG-541, we focused on earlier time points. Many PROTACs induce a distinct target degradation within four hours [5–7]. At this time point, seven proteins showed a decreased expression with a log2 fold change < -1 (Fig. 2D, STable2). Two of these proteins, G1 To S Phase Transition 1 (GSPT1, eRF3a) and GSPT2 (eRF3b), components of the eRF1-eFR3-guanosine triphosphate (GTP) translation termination complex [24], were shown to be CRBN neosubstrates [25–28]. Therefore, we investigated the effects of MDEG-541 on eRF3 in greater detail. The pancreatic cancer cell line KP4 is the most MDEG-541 sensitive. Upon the treatment with MDEG-541, GSPT1/2 expression was decreased after 3 h. This was followed by reduced expression of MYC after 12 h (Fig. 2E). Hereby, regulation of GSPT1, GSPT2, and MYC occurs in a dose dependent

fashion (SFig. 4A). Also, in PSN1 and HCT116 cells, downregulation of GSPT1/2 protein expression by MDEG-541 occurred before the reduced expression of MYC (SFig. 4B and 4C). HCT116 do not express GSPT2 and therefore, the protein was not detected by western blot. Furthermore, neither *GSPT1* nor *MYC* mRNA expression was decreased in MDEG-541 treated HCT116 cells (SFig. 4D). The reduced expression of GSPT1/2 induced by MDEG-541 was rescued by blocking the ubiquitination machinery (SFig. 4E) and the proteasome (SFig. 4F). In addition, regulation of GSPT1/2 was dependent on CRBN in PSN1 and HCT116 cells (SFig. 4G). In sum, MDEG-541 regulates MYC and the eRF3 components GSPT1 and GSPT2 in a ubiquitination-, Cereblon-, and proteasome dependent manner.

3.5. *Effects of GSPT1 degraders CC-885 and CC-90009*

Work from 2016 showed that GSPT1 is a CRBN neosubstrate and the CELMoD CC-885, a compound with activity against AML, triggers GSPT1 degradation [25]. Accessing a functional CRISPR-Cas drop out screen [19], we detected that especially *GSPT1* is a relevant fitness factor for colon and pancreatic cancer cells with similar scores as detected in AML (SFig. 4H). Therefore, we used CC-885 to investigate the regulation of GSPT1 and MYC. CC-885 downregulated GSPT1 and GSPT2 expression (Fig. 3A). Furthermore, CC-885 downregulated expression of MYC (Fig. 3A). Again, CC-885-mediated regulation of all proteins was dependent on the proteasome (SFig. 5A) and the ubiquitination machinery (SFig. 5B). Compared to KP4 cells, HCT-116 and PSN1 cells are less sensitive to CC-885 (Fig. 3B). Therefore, we concluded that with respect to the investigated changes, CC-885 mimics

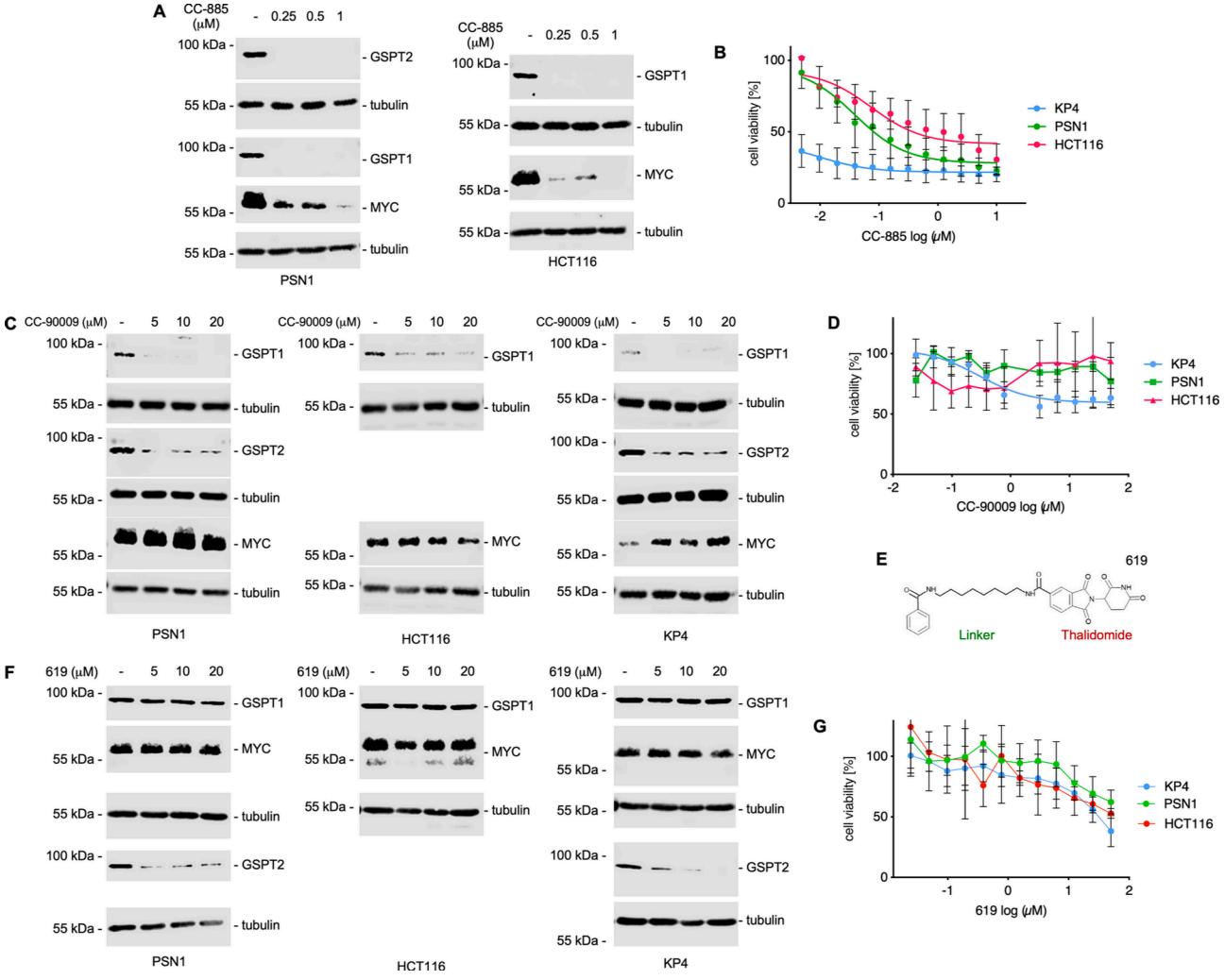

Fig. 3. *Phenotypes induced by the CELMoDs CC-885 and CC-90009.* A GSPT2, GSPT1 and MYC western blot of PSN1 (left panel) or GSPT1 and MYC western blot of HCT116 (right panel) cells treated for 24 h with 0.25 μM, 0.5 μM and 1 μM CC-885 or DMSO vehicle control. Tubulin: loading control. Shown is one representative experiment out of three independent biological replicates. B HCT116, PSN1, and KP4 cells were treated for 72 h with the indicated concentrations of CC-885. Viability was measured with MTT assays and vehicle treated controls were arbitrarily set to 100%. Experiment was performed three times as biological replicates conducted as technical triplicates. Shown is the mean ± S.D. C GSPT2, GSPT1 and MYC western blot of PSN1 and KP4 (left panel and right panel) or GSPT1 and MYC western blot of HCT116 (middle panel) cells treated for 24 h with 5 μM, 10 μM, and 20 μM of CC-90009 or DMSO vehicle control. Tubulin: loading control. Shown is one representative experiment out of three independent biological replicates. D HCT116, PSN1, and KP4 cells were treated for 72 h with the indicated concentrations of CC-90009. Viability was measured with MTT assays and vehicle treated controls were arbitrarily set to 100%. Experiment was performed three times as biological replicates conducted as technical triplicates. Shown is the mean ± S.D. E Sructure of compound 619. F GSPT2, GSPT1 and MYC western blot of PSN1 and KP4 (left panel and right panel) or GSPT1 and MYC western blot of HCT116 (middle panel) cells treated for 24 h with 5 μM, 10 μM, and 20 μM of compound 619 or DMSO vehicle control. Tubulin: loading control. Shown is one representative experiment out of three independent biological replicates. G HCT116, PSN1, and KP4 cells were treated for 72 h with the indicated concentrations of compound 619. Viability was measured with MTT assays and vehicle treated controls were arbitrarily set to 100%. Experiment was performed three times as biological replicates conducted as technical triplicates. Shown is the mean ± S.D.

MDEG-541. The clinical development of CC-885 was hampered by toxicities associated with various targets [28–31]. To further corroborate the contribution of GSPT1 to the cellular effects of MDEG-541, we used the specific GSPT1 degrader CC-90009 [29]. Indeed, CC-90009 induced the degradation of GSPT1 and GSPT2 (Fig. 3C). However, MYC expression was not changed by the inhibitor (Fig. 3C). Furthermore, compared to MDEG-541 and CC-885, the specific GSPT1/2 degrader showed a distinctly reduced cellular activity in the investigated cell lines (Fig. 3D). In order to test whether both parts of MDEG-541 are needed for the observed responses, we synthesized compound 619, containing Thalidomide and the linker of MDEG-541, but not the 10058-F4 part (Fig. 3E). Interestingly, 619 induced the degradation of GSPT2, but not GSPT1 or MYC (Fig. 3F), pointing to a possibility to achieve selectivity. Furthermore, compared to MDEG-541, the cellular activity of 619 is reduced (Fig. 3G). In sum, these data were interpreted, that MYC regulation and cellular activity might involve an additional CRBN neosubstrate.

3.6. MDEG-541 controls PLK1 expression

The CELMoD CC-885 was recently demonstrated to induce ubiquitination and degradation of the cell cycle promoting kinase PLK1 [31]. Since PLK1 was demonstrated to regulate protein expression of MYC family members [32–35], we investigated the impact of MDEG-541 on a potential PLK1-MYC pathway. Indeed, MDEG-541 reduced the expression of PLK1 in a dose-dependent fashion (Fig. 4A). Hereby, the PLK1 degradation kinetics followed the kinetics described for MYC and PLK1 expression was completely lost after 24 h (Fig. 4B). Also, in KP4 cells, MDEG-541 clearly regulated PLK1 expression (SFig. 6A). MDEG-541-mediated regulation of PLK1 was again dependent on CRBN (SFig. 6B), the proteasome (SFig. 6C), and the ubiquitination machinery (SFig. 6D). *PLK1* mRNA is not regulated by MDEG-541 (SFig. 6E). In contrast to CC-885, the GSPT1 degrader CC-90009 does not regulate PLK1 (Fig. 4C).

To test whether PLK1 might be upstream of MYC, we used the specific PLK1 inhibitor Volasertib. With GI_{50} values of 0.19 μM for PSN1 and 0.17 μM for HCT116, both cell lines are sensitive to the inhibitor

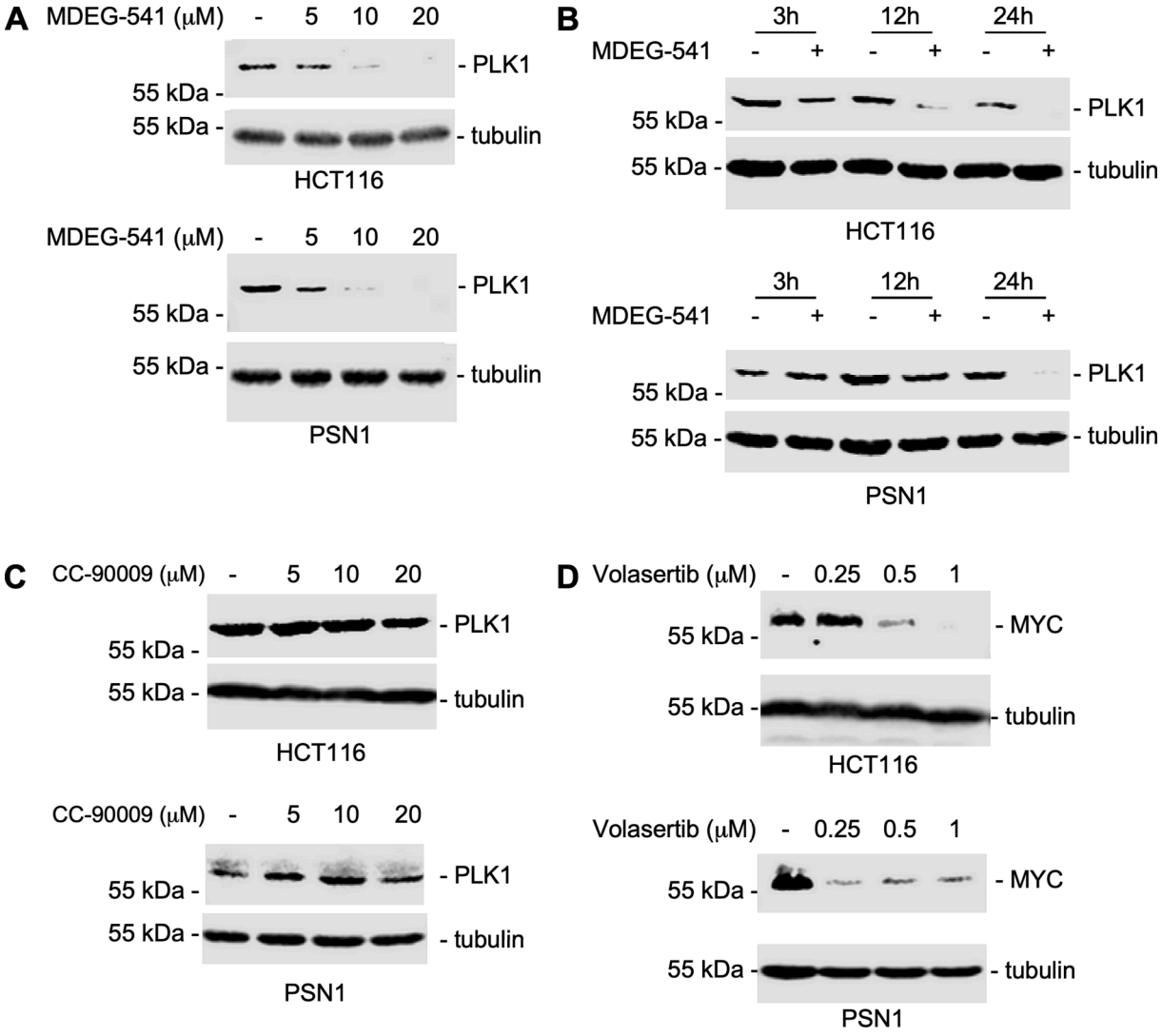

Fig. 4. *PLK1 expression is regulated by MDEG-541.* A PLK1 western blot of HCT116 (upper panel) and PSN1 (lower panel) cells treated for 24 h with 5 μM, 10 μM, and 20 μM of MDEG-541 or DMSO vehicle control. Tubulin: loading control. Shown is one representative experiment out of three independent biological replicates. B PLK1 western blot of HCT116 (upper panel) and PSN1 (lower panel) cells treated treated for 3 h, 12 h, or 24 h with 10 μM MDEG-541 or DMSO vehicle control. Tubulin: loading control. Shown is one representative experiment out of three independent biological replicates. C PLK1 western blot of HCT116 (upper panel) and PSN1 (lower panel) cells treated for 24 h with the indicated concentrations of CC-90009 or DMSO vehicle control. Tubulin: loading control. Shown is one representative experiment out of three independent biological replicates. D MYC western blot of HCT116 (upper panel) and PSN1 (lower panel) cells treated for 24 h with the indicated concentrations of Volasertib or DMSO vehicle control. Tubulin: loading control. Shown is one representative experiment out of three independent biological replicates.

(SFig. 6F). After 24 h of treatment with Volasertib, MYC expression was reduced in HCT116 and PSN1 cells (Fig. 4D). Together these results suggest, that MDEG-541 controls PLK1 in addition to MYC and GSPT1/2.

4. Discussion

We intended to develop a MYC PROTAC by combining the 10058-F4 [15] derivative 28RH to Thalidomide [16]. Out of several potential degraders, we selected MDEG-541 for further characterization due to reduced MYC expression and cellular activity. We provide evidence that MDEG-541 diminished the expression of cancer-relevant molecules like MYC, GSPT1/2, and PLK1 in an ubiquitin-, CRBN-, and proteasome-dependent fashion. The loss of viability induced by MDEG-541 is therefore most likely due to the pleiotropic mode of action.

In the simplest case, the development of a PROTAC requires a ubiquitin ligase E3 recruiting and a target protein ligand, as well as a linker of suitable length and hydrophilicity [36]. However, several groups have shown that the design of PROTACs is much more nuanced in terms of both junction geometry and ligand targeting the substrate being in the focus [37–39]. Terms like the substitution pattern of the E3-ligase and the substrate binding ligands moreover play a significant role. The basis of selectivity relies on protein-protein interactions between the E3 ubiquitin ligase and the target protein, leading to stable ternary complexes and efficient degradation of the target [37–39]. Given their modular design, studies have shown that PROTACs are adjustable and changes in all three PROTAC components - target protein ligand, linker and E3 ligand - can have a profound impact on their potency and efficacy [36]. We prepared a series of different small molecules resulting from the connection of 10058-F4 derivative as a MYC inhibitor with Thalidomide as an E3 ligase binding sequence, using alkyl-linkers of different length. Within this set of compounds, MDEG-541 showed in the first screening experiments a dose-dependent reduction of viability, efficacy in the single digit μM range in conventional cell lines and primary patient-derived organoids, and an ubiquitin-, proteasome-, and Cereblon-dependent MYC regulation.

Due to the rather prolonged MYC degradation kinetics induced by MDEG-541, we investigated other potential targets and show that MDEG-541 induced GSPT1/2 as well as PLK1 degradation. GSPT1 is a common CRBN neosubstrate and degradation is induced by CELMoDs, like CC-885 [25], BTX306 [40], or CC-90009 [29], or as an off-target in the framework of different CRBN-based PROTAC concepts, aiming to target MDM2 [27], JAK2 [41] or receptor tyrosine kinases (RTKs) [26]. Since we detected no regulation of MYC and PLK1 by the specific GSPT1 and GSPT2 degrader CC-90009 [29], which was accompanied by minimal cellular responsiveness, the contribution of GSPT1 or GSPT2 to the described MDEG-541 induced phenotypes might be neglectable. However, we cannot exclude that GSPT1/2 is important in context of the regulation of other targets, whose expression is regulated by MDEG-541.

The CELMoD CC-885 was recently demonstrated to induce ubiquitination and degradation of the cell cycle promoting kinase PLK1 [31]. Hereby, CC-885 induces the direct interaction of CRBN with PLK1 [31]. Consistently, we observed that MDEG-541 regulates PLK1 dependent on ubiquitylation. CC-885 induced degradation in A549 cells occurs within two to four hours [31]. In contrast, MDEG-541 treatment results in a prolonged PLK1 degradation kinetics, which follows the kinetics observed for MYC. Although treatment with the PLK1 inhibitor Volasertib point to the possibility that PLK1 might act upstream of MYC, we cannot exclude that a Volasertib off-target contributes to the observed effects. Therefore, the mode of regulation of both - MYC and PLK1 - by MDEG-541 remains incompletely understood and demands further investigations. Direct analyzing ubiquitylation of the described targets as well as studying their direct interaction with CRBN will be needed, to further characterize the mode of action of MDEG-541.

The further development of MDEG-541 might be limited by toxicities. For example, the clinical development of CC-885 was hampered by significant toxicities associated with various off-targets [28–31]. In our proteome analysis additional potential off-targets were detected. Although the analysis of primary human fibroblasts argues for the existence of a therapeutic window, it remains unclear whether such a window can be therapeutically engaged *in vivo*.

In attempts to test whether the 10058-F4 component is needed for the molecular activity of MDEG-541, we synthesized compound 619, containing Thalidomide and the linker of MDEG-541. The cellular activity as well as the degradation inducing properties of this compound are diminished. Therefore, the complete MDEG-541 molecule is needed to trigger the described molecular and cellular responses. Whether a different linker design allows to develop a compound with similar activity as MDEG-541, but without the 10058-F4 component, awaits further experimentation.

5. Conclusion

In sum, we have characterized a novel compound with a MYC-MAX dimerization inhibitor 10058-F4 derivative 28RH warhead linked to the CRBN-binder IMiD Thalidomide. We provide evidence for a MDEG-541 sensitive subgroup of gastrointestinal cancers and show that MDEG-541 controls expression of relevant cancer targets, including MYC, GSPT1/2, and PLK1. Therefore, MDEG-541 might broaden opportunities to target these molecules.

Declaration of Competing Interest

The authors declare the following financial interests/personal relationships which may be considered as potential competing interests: The funding agencies had no influence on any aspect of the study. B.Ku. is co-founder and shareholder of msAId GmbH and OmicScouts GmbH. B.Ku. has no operational role in either company. The authors declare no further potential conflicts of interest.

Acknowledgements

We thank all the patients providing tissue for the generation of primary tumor models. This work was supported by the Wilhelm Sander Stiftung (Grant 2016.004.1 to G.S. and S.M., 2017.048.2 to G.S., and 2019.086.1 to G.S.), Deutsche Forschungsgemeinschaft (DFG) (SCHN959/3-2 and SCHN959/6-1 to G.S., SFB1321 (Project-ID 329628492) P13 to G.S. and S01 to G.S., D.S., M.R.), and Deutsche Krebshilfe (70113760 to G.S.; Max Eder Program 111273 to M.R.).

Appendix A. Supplementary material

Supplementary data to this article can be found online at https://doi.org/10.1016/j.bioorg.2021.105505.

References

[1] M. Schapira, M.F. Calabrese, A.N. Bullock, C.M. Crews, Targeted protein degradation: expanding the toolbox, Nat. Rev. Drug Discov. 18 (12) (2019) 949–963, https://doi.org/10.1038/s41573-019-0047-y.

[2] P.P. Chamberlain, L.G. Hamann, Development of targeted protein degradation therapeutics, Nat. Chem. Biol. 15 (10) (2019) 937–944, https://doi.org/10.1038/s41589-019-0362-y.

[3] R. Verma, D. Mohl, R.J. Deshaies, Harnessing the Power of Proteolysis for Targeted Protein Inactivation, Mol. Cell 77 (3) (2020) 446–460, https://doi.org/10.1016/j.molcel.2020.01.010.

[4] G.M. Burslem, C.M. Crews, Proteolysis-Targeting Chimeras as Therapeutics and Tools for Biological Discovery, Cell 181 (1) (2020) 102–114, https://doi.org/10.1016/j.cell.2019.11.031.

[5] G.E. Winter, D.L. Buckley, J. Paulk, J.M. Roberts, A. Souza, S. Dhe-Paganon, J. E. Bradner, Phthalimide conjugation as a strategy for in vivo target protein degradation, Science 348 (6241) (2015) 1376–1381, https://doi.org/10.1126/science:aab1433.

[6] J. Salami, S. Alabi, R.R. Willard, N.J. Vitale, J. Wang, H. Dong, M. Jin, D. P. McDonnell, A.P. Crew, T.K. Neklesa, C.M. Crews, Androgen receptor degradation by the proteolysis-targeting chimera ARCC-4 outperforms

enzalutamide in cellular models of prostate cancer drug resistance, Commun. Biol. 1 (2018) 100, https://doi.org/10.1038/s42003-018-0105-8.
[7] B. Adhikari, J. Bozilovic, M. Diebold, J.D. Schwarz, J. Hofstetter, M. Schröder, M. Wanior, A. Narain, M. Vogt, N. Dudvarski Stankovic, A. Baluapuri, L. Schönemann, L. Eing, P. Bhandare, B. Kuster, A. Schlosser, S. Heinzlmeir, C. Sotriffer, S. Knapp, E. Wolf, PROTAC-mediated degradation reveals a non-catalytic function of AURORA-A kinase, Nat. Chem. Biol. 16 (11) (2020) 1179–1188, https://doi.org/10.1038/s41589-020-00652-y.
[8] G. Lu, R.E. Middleton, H. Sun, M. Naniong, C.J. Ott, C.S. Mitsiades, K.-K. Wong, J. E. Bradner, W.G. Kaelin, The Myeloma Drug Lenalidomide Promotes the Cereblon-Dependent Destruction of Ikaros Proteins, Science 343 (6168) (2014) 305–309, https://doi.org/10.1126/science:1244917.
[9] J. Krönke, N.D. Udeshi, A. Narla, P. Grauman, S.N. Hurst, M. McConkey, T. Svinkina, D. Heckl, E. Comer, X. Li, C. Ciarlo, E. Hartman, N. Munshi, M. Schenone, S.L. Schreiber, S.A. Carr, B.L. Ebert, Lenalidomide Causes Selective Degradation of IKZF1 and IKZF3 in Multiple Myeloma Cells, Science 343 (6168) (2014) 301–305, https://doi.org/10.1126/science:1244851.
[10] J. Krönke, E.C. Fink, P.W. Hollenbach, K.J. MacBeth, S.N. Hurst, N.D. Udeshi, P. P. Chamberlain, D.R. Mani, H.W. Man, A.K. Gandhi, T. Svinkina, R.K. Schneider, M. McConkey, M. Järås, E. Griffiths, M. Wetzler, L. Bullinger, B.E. Cathers, S. A. Carr, R. Chopra, B.L. Ebert, Lenalidomide induces ubiquitination and degradation of CK1α in del(5q) MDS, Nature 523 (7559) (2015) 183–188, https://doi.org/10.1038/nature14610.
[11] S.A. Holstein, J. Hillengass, P.L. McCarthy, Next-Generation Drugs Targeting the Cereblon Ubiquitin Ligase, J. Clin. Oncol. 36 (20) (2018) 2101–2104, https://doi.org/10.1200/JCO.2018.77.9637.
[12] M. Wirth, S. Mahboobi, O.H. Krämer, G. Schneider, Concepts to Target MYC in Pancreatic Cancer, Mol. Cancer Ther. 15 (8) (2016) 1792–1798, https://doi.org/10.1158/1535-7163.MCT-16-0050.
[13] E. Wolf, M. Eilers, Targeting MYC Proteins for Tumor Therapy, Annu. Rev. Cancer Biol. 4 (1) (2020) 61–75, https://doi.org/10.1146/annurev-cancerbio-030518-055826.
[14] B.L. Allen-Petersen, R.C. Sears, Mission Possible: Advances in MYC Therapeutic Targeting in Cancer, Biodrugs 33 (2019) 539–553, https://doi.org/10.1007/s40259-019-00370-5.
[15] X. Yin, C. Giap, J.S. Lazo, E.V. Prochownik, Low molecular weight inhibitors of Myc-Max interaction and function, Oncogene 22 (40) (2003) 6151–6159, https://doi.org/10.1038/sj.onc.1206641.
[16] T. Ito, H. Ando, T. Suzuki, T. Ogura, K. Hotta, Y. Imamura, Y. Yamaguchi, H. Handa, Identification of a Primary Target of Thalidomide Teratogenicity, Science 327 (5971) (2010) 1345–1350, https://doi.org/10.1126/science:1177319.
[17] N. Gerstner, T. Kehl, K. Lenhof, A. Müller, C. Mayer, L. Eckhart, N.L. Grammes, C. Diener, M. Hart, O. Hahn, J. Walter, T. Wyss-Coray, E. Meese, A. Keller, H.-P. Lenhof, GeneTrail 3: advanced high-throughput enrichment analysis, Nucleic Acids Res. 48 (2020), https://doi.org/10.1093/nar/gkaa306.
[18] M. Ghandi, F.W. Huang, J. Jané-Valbuena, G.V. Kryukov, C.C. Lo, E.R. McDonald, J. Barretina, E.T. Gelfand, C.M. Bielski, H. Li, K. Hu, A.Y. Andreev-Drakhlin, J. Kim, J.M. Hess, B.J. Haas, F. Aguet, B.A. Weir, M.V. Rothberg, B.R. Paolella, M. S. Lawrence, R. Akbani, Y. Lu, H.L. Tiv, P.C. Gokhale, A. de Weck, A.A. Mansour, C. Oh, J. Shih, K. Hadi, Y. Rosen, J. Bistline, K. Venkatesan, A. Reddy, D. Sonkin, M. Liu, J. Lehar, J.M. Korn, D.A. Porter, M.D. Jones, J. Golji, G. Caponigro, J. E. Taylor, C.M. Dunning, A.L. Creech, A.C. Warren, J.M. McFarland, M. Zamanighomi, A. Kauffmann, N. Stransky, M. Imielinski, Y.E. Maruvka, A. D. Cherniack, A. Tsherniak, F. Vazquez, J.D. Jaffe, A.A. Lane, D.M. Weinstock, C. M. Johannessen, M.P. Morrissey, F. Stegmeier, R. Schlegel, W.C. Hahn, G. Getz, G. B. Mills, J.S. Boehm, T.R. Golub, L.A. Garraway, W.R. Sellers, Next-generation characterization of the Cancer Cell Line Encyclopedia, Nature 569 (7757) (2019) 503–508, https://doi.org/10.1038/s41586-019-1186-3.
[19] R.M. Meyers, J.G. Bryan, J.M. McFarland, B.A. Weir, A.E. Sizemore, H. Xu, N. V. Dharia, P.G. Montgomery, G.S. Cowley, S. Pantel, A. Goodale, Y. Lee, L.D. Ali, G. Jiang, R. Lubonja, W.F. Harrington, M. Strickland, T. Wu, D.C. Hawes, V. A. Zhivich, M.R. Wyatt, Z. Kalani, J.J. Chang, M. Okamoto, K. Stegmaier, T. R. Golub, J.S. Boehm, F. Vazquez, D.E. Root, W.C. Hahn, A. Tsherniak, Computational correction of copy number effect improves specificity of CRISPR–Cas9 essentiality screens in cancer cells, Nat. Genet. 49 (12) (2017) 1779–1784, https://doi.org/10.1038/ng.3984.
[20] M.L. Hyer, M.A. Milhollen, J. Ciavarri, P. Fleming, T. Traore, D. Sappal, J. Huck, J. Shi, J. Gavin, J. Brownell, Y.u. Yang, B. Stringer, R. Griffin, F. Bruzzese, T. Soucy, J. Duffy, C. Rabino, J. Riceberg, K. Hoar, A. Lublinsky, S. Menon, M. Sintchak, N. Bump, S.M. Pulukuri, S. Langston, S. Tirrell, M. Kuranda, P. Veiby, J. Newcomb, P. Li, J.T. Wu, J. Powe, L.R. Dick, P. Greenspan, K. Galvin, M. Manfredi, C. Claiborne, B.S. Amidon, N.F. Bence, A small-molecule inhibitor of the ubiquitin activating enzyme for cancer treatment, Nat. Med. 24 (2) (2018) 186–193, https://doi.org/10.1038/nm.4474.
[21] K. Raina, J. Lu, Y. Qian, M. Altieri, D. Gordon, A.M.K. Rossi, J. Wang, X. Chen, H. Dong, K. Siu, J.D. Winkler, A.P. Crew, C.M. Crews, K.G. Coleman, PROTAC-induced BET protein degradation as a therapy for castration-resistant prostate cancer, Proc. National Acad. Sci. 113 (26) (2016) 7124–7129, https://doi.org/10.1073/pnas.1521738113.
[22] G. Vlachogiannis, S. Hedayat, A. Vatsiou, Y. Jamin, J. Fernández-Mateos, K. Khan, A. Lampis, K. Eason, I. Huntingford, R. Burke, M. Rata, D.-M. Koh, N. Tunariu, D. Collins, S. Hulkki-Wilson, C. Ragulan, I. Spiteri, S.Y. Moorcraft, I. Chau, S. Rao, D. Watkins, N. Fotiadis, M. Bali, M. Darvish-Damavandi, H. Lote, Z. Eltahir, E. C. Smyth, R. Begum, P.A. Clarke, J.C. Hahne, M. Dowsett, J. de Bono, P. Workman, A. Sadanandam, M. Fassan, O.J. Sansom, S. Eccles, N. Starling, C. Braconi, A. Sottoriva, S.P. Robinson, D. Cunningham, N. Valeri, Patient-derived organoids model treatment response of metastatic gastrointestinal cancers, Science 359 (6378) (2018) 920–926, https://doi.org/10.1126/science:aao2774.
[23] A. Liberzon, C. Birger, H. Thorvaldsdóttir, M. Ghandi, J. Mesirov, P. Tamayo, The Molecular Signatures Database Hallmark Gene Set Collection, Cell Syst. 1 (6) (2015) 417–425, https://doi.org/10.1016/j.cels.2015.12.004.
[24] C.U.T. Hellen, Translation Termination and Ribosome Recycling in Eukaryotes, Csh Perspect. Biol. 10 (2018), a032656, https://doi.org/10.1101/cshperspect.a032656.
[25] M.E. Matyskiela, G. Lu, T. Ito, B. Pagarigan, C.-C. Lu, K. Miller, W. Fang, N.-Y. Wang, D. Nguyen, J. Houston, G. Carmel, T. Tran, M. Riley, L. Nosaka, G. C. Lander, S. Gaidarova, S. Xu, A.L. Ruchelman, H. Handa, J. Carmichael, T. O. Daniel, B.E. Cathers, A. Lopez-Girona, P.P. Chamberlain, A novel cereblon modulator recruits GSPT1 to the CRL4CRBN ubiquitin ligase, Nature 535 (7611) (2016) 252–257, https://doi.org/10.1038/nature18611.
[26] M. Ishoey, S. Chorn, N. Singh, M.G. Jaeger, M. Brand, J. Paulk, S. Bauer, M.A. Erb, K. Parapatics, A.C. Müller, K.L. Bennett, G.F. Ecker, J.E. Bradner, G.E. Winter, Translation Termination Factor GSPT1 Is a Phenotypically Relevant Off-Target of Heterobifunctional Phthalimide Degraders, ACS Chem. Biol. 13 (2018) 553–560. 10.1021/acschembio.7b00969.
[27] J. Yang, Y. Li, A. Aguilar, Z. Liu, C.-Y. Yang, S. Wang, Simple Structural Modifications Converting a Bona fide MDM2 PROTAC Degrader into a Molecular Glue Molecule: A Cautionary Tale in the Design of PROTAC Degraders, J. Med. Chem. 62 (2019) 9471–9487, https://doi.org/10.1021/acs.jmedchem.9b00846.
[28] C.E. Powell, G. Du, J. Che, Z. He, K.A. Donovan, H. Yue, E.S. Wang, R.P. Nowak, T. Zhang, E.S. Fischer, N.S. Gray, Selective Degradation of GSPT1 by Cereblon Modulators Identified via a Focused Combinatorial Library, ACS Chem. Biol. 15 (10) (2020) 2722–2730, https://doi.org/10.1021/acschembio.0c00520.s001.
[29] C. Surka, L. Jin, N. Mbong, C.-C. Lu, I.S. Jang, E. Rychak, D. Mendy, T. Clayton, E. A. Tindall, C. Hsu, C. Fontanillo, E. Tran, A. Contreras, S.-W.-K. Ng, M. E. Matyskiela, K. Wang, P.P. Chamberlain, B. Cathers, J. Carmichael, J.D. Hansen, J.C.Y. Wang, M.D. Minden, J. Fan, D.W. Pierce, M. Pourdehnad, M. Rolfe, A. Lopez-Girona, J.E. Dick, G. Lu, CC-90009, a novel cereblon E3 ligase modulator targets acute myeloid leukemia blasts and leukemia stem cells, Blood 137 (2020) 661–677, https://doi.org/10.1182/blood.2020008676.
[30] B.-B. Hao, X.-J. Li, X.-L. Jia, Y.-X. Wang, L.-H. Zhai, D.-Z. Li, J. Liu, D. Zhang, Y.-l. Chen, Y.-h. Xu, S.-K. Lee, G.-F. Xu, X.-H. Chen, Y.-J. Dang, B. Liu, M.-J. Tan, The novel cereblon modulator CC-885 inhibits mitophagy via selective degradation of BNIP3L, Acta Pharmacol. Sin. 41 (9) (2020) 1246–1254, https://doi.org/10.1038/s41401-020-0367-9.
[31] L. Li, W. Xue, Z. Shen, J. Liu, M. Hu, Z. Cheng, Y. Wang, Y. Chen, H. Chang, Y. Liu, B. Liu, J. Zhao, A Cereblon Modulator CC-885 Induces CRBN- and p97-Dependent PLK1 Degradation and Synergizes with Volasertib to Suppress Lung Cancer, Mol. Ther. - Oncolytics. 18 (2020) 215–225, https://doi.org/10.1016/j.omto.2020.06.013.
[32] J. Tan, Z. Li, P.L. Lee, P. Guan, M.Y. Aau, S.T. Lee, M. Feng, C.Z. Lim, E.Y.J. Lee, Z. N. Wee, Y.C. Lim, R.K.M. Karuturi, Q. Yu, PDK1 Signaling Toward PLK1–MYC Activation Confers Oncogenic Transformation, Tumor-Initiating Cell Activation, and Resistance to mTOR-Targeted Therapy, Cancer Discov. 3 (10) (2013) 1156–1171, https://doi.org/10.1158/2159-8290.CD-12-0595.
[33] D. Xiao, M. Yue, H. Su, P. Ren, J. Jiang, F. Li, Y. Hu, H. Du, H. Liu, G. Qing, Polo-like Kinase-1 Regulates Myc Stabilization and Activates a Feedforward Circuit Promoting Tumor Cell Survival, Mol. Cell 64 (3) (2016) 493–506, https://doi.org/10.1016/j.molcel.2016.09.016.
[34] Y. Ren, C. Bi, X. Zhao, T. Lwin, C. Wang, J. Yuan, A.S. Silva, B.D. Shah, B. Fang, T. Li, J.M. Koomen, H. Jiang, J.C. Chavez, L. Pham, P.R. Sudalagunta, L. Wan, X. Wang, W.S. Dalton, L.C. Moscinski, K.H. Shain, J. Vose, J.L. Cleveland, E.M. Sotomayor, K. Fu, J. Tao, PLK1 stabilizes a MYC-dependent kinase network in aggressive B cell lymphomas, J. Clin. Invest. 128 (2018) 5517–5530. 10.1172/jci122533.
[35] D. Wang, A. Pierce, B. Veo, S. Fosmire, E. Danis, A. Donson, S. Venkataraman, R. Vibhakar, A Regulatory Loop of FBXW7-MYC-PLK1 Controls Tumorigenesis of MYC-Driven Medulloblastoma, Cancers. 13 (2021) 387, https://doi.org/10.3390/cancers13030387.
[36] J. Hines, S. Lartigue, H. Dong, Y. Qian, C.M. Crews, MDM2-recruiting PROTAC Offers Superior, Synergistic Anti-proliferative Activity via Simultaneous Degradation of BRD4 and Stabilization of p53, Cancer Res. 79 (2018) canres.2918.2018. 10.1158/0008-5472.can-18-2918.
[37] D.P. Bondeson, B.E. Smith, G.M. Burslem, A.D. Buhimschi, J. Hines, S. Jaime-Figueroa, J. Wang, B.D. Hamman, A. Ishchenko, C.M. Crews, Lessons in PROTAC Design from Selective Degradation with a Promiscuous Warhead, Cell Chem. Biol. 25 (1) (2018) 78–87.e5, https://doi.org/10.1016/j.chembiol.2017.09.010.
[38] D.L. Buckley, K. Raina, N. Darricarrere, J. Hines, J.L. Gustafson, I.E. Smith, A. H. Miah, J.D. Harling, C.M. Crews, HaloPROTACS: Use of Small Molecule PROTACs to Induce Degradation of HaloTag Fusion Proteins, ACS Chem. Biol. 10 (2015) 1831–1837, https://doi.org/10.1021/acschembio.5b00442.
[39] M.S. Gadd, A. Testa, X. Lucas, K.-H. Chan, W. Chen, D.J. Lamont, M. Zengerle, A. Ciulli, Structural basis of PROTAC cooperative recognition for selective protein

degradation, Nat. Chem. Biol. 13 (5) (2017) 514–521, https://doi.org/10.1038/nchembio.2329.

[40] J. Zou, R.J. Jones, H. Wang, I. Kuiatse, F. Shirazi, E.E. Manasanch, H.C. Lee, R. Sullivan, L. Fung, N. Richard, P. Erdman, E. Torres, D. Hecht, I. Lam, B. McElwee, A.H. Chourasia, K.W.H. Chan, F. Mercurio, D.I. Stirling, R.Z. Orlowski, The novel protein homeostatic modulator BTX306 is active in myeloma and overcomes bortezomib and lenalidomide resistance, J. Mol. Med. 98 (8) (2020) 1161–1173, https://doi.org/10.1007/s00109-020-01943-6.

[41] Y. Chang, J. Min, J. Jarusiewicz, M. Actis, S.-Y.-C. Bradford, A. Mayasundari, L. Yang, D. Chepyala, L.J. Alcock, K.G. Roberts, S. Nithianantham, D. Maxwell, L. Rowland, R. Larsen, A. Seth, H. Goto, T. Imamura, K. Akahane, B. Hansen, S. M. Pruett-Miller, E.M. Paietta, M.R. Litzow, C. Qu, J.J. Yang, M. Fischer, Z. Rankovic, C.G. Mullighan, Degradation of Janus kinases in CRLF2- rearranged acute lymphoblastic leukemia, Blood (2021), https://doi.org/10.1182/blood.2020006846.

Update

Bioorganic Chemistry
Volume 146, Issue , May 2024, Page

DOI: https://doi.org/10.1016/j.bioorg.2024.107248

Bioorganic Chemistry 146 (2024) 107248

Contents lists available at ScienceDirect

Bioorganic Chemistry

journal homepage: www.elsevier.com/locate/bioorg

Corrigendum

Corrigendum to "A novel Cereblon E3 ligase modulator with antitumor activity in gastrointestinal cancer" [Bioorgan. Chem. 119 (2022) 105505]

Svenja Lier [a,1], Andreas Sellmer [b,1], Felix Orben [a], Stephanie Heinzlmeir [c], Lukas Krauß [a], Christian Schneeweis [a], Zonera Hassan [a], Carolin Schneider [a], Arlette Schäfer [a], Herwig Pongratz [b], Thomas Engleitner [d], Rupert Öllinger [d], Anna Kuisl [e], Florian Bassermann [e,f], Christoph Schlag [a], Bo Kong [g,h], Stefan Dove [b], Bernhard Kuster [c,f,i], Roland Rad [d,f], Maximilian Reichert [a,f,j], Matthias Wirth [k], Dieter Saur [f,l], Siavosh Mahboobi [b,*], Günter Schneider [a,m,*]

[a] *Medical Clinic and Policlinic II, Klinikum Rechts der Isar, TU Munich, 81675 Munich, Germany*
[b] *Institute of Pharmacy, Faculty of Chemistry and Pharmacy, University of Regensburg, 93040 Regensburg, Germany*
[c] *Chair of Proteomics and Bioanalytics, TU Munich, 85354 Freising, Germany*
[d] *Institute of Molecular Oncology and Functional Genomics, MRI, TU Munich, Germany*
[e] *Medical Clinic and Policlinic III, Klinikum Rechts der Isar, TU Munich, 81675 Munich, Germany*
[f] *German Cancer Research Center (DKFZ) and German Cancer Consortium (DKTK), 69120 Heidelberg, Germany*
[g] *Department of Surgery, Klinikum Rechts der Isar, TU Munich, 81675 Munich, Germany*
[h] *Department of General Surgery, University of Ulm, 89081 Ulm, Germany*
[i] *Bavarian Center for Biomolecular Mass Spectrometry (BayBioMS), TU Munich, 85354 Freising, Germany*
[j] *Center for Protein Assemblies (CPA), Technische Universität München, 85747 Garching, Germany*
[k] *Department of Hematology, Oncology and Cancer Immunology, Campus Benjamin Franklin, Charíte – Universitätsmedizin Berlin, 12203 Berlin, Germany*
[l] *Institute for Translational Cancer Research and Experimental Cancer Therapy, Klinikum Rechts der Isar, TU Munich, Germany*
[m] *University Medical Center Göttingen, Department of General, Visceral and Pediatric Surgery, 37075 Göttingen, Germany*

The original article reports the structure of MDEG-541. Regrettably, Figure 1A contains an inaccurately depicted chemical structure due to an error. The correct structure of MDEG-541 is shown below.

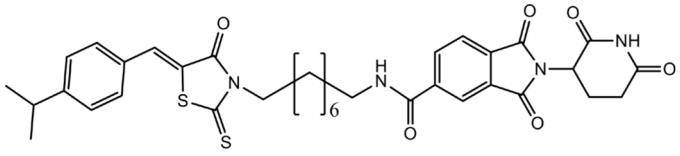

MDEG-541

(*Z*)-2-(2,6-dioxopiperidin-3-yl)-*N*-(3-(5-(4-isopropylbenzylidene)-4-oxo-2-thioxothiazolidin-3-yl)propyl)-1,3-dioxoisoindoline-5-carboxamide

This error does not affect the conclusions of the manuscript, since the correct compound was used in all experiments. We deeply regret the error and apologize for any confusion the error may have caused.

DOI of original article: https://doi.org/10.1016/j.bioorg.2021.105505.

* Corresponding authors at: University Medical Center Göttingen, Department of General, Visceral and Pediatric Surgery, 37075 Göttingen and Klinikum rechts der Isar, Technische Universität München, 81675 Munich, Germany (G. Schneider). Institute of Pharmacy, Faculty of Chemistry and Pharmacy, University of Regensburg, 93040 Regensburg, Germany (S. Mahboobi).
E-mail addresses: siavosh.mahboobi@ur.de (S. Mahboobi), guenter.schneider@med.uni-goettingen.de (G. Schneider).
[1] Equally contributing first authors.

https://doi.org/10.1016/j.bioorg.2024.107248

Available online 7 March 2024